

Ultra-high sensitivity magnetic field and magnetization measurements with an atomic magnetometer

H. B. Dang¹ and A.C. Maloof² and M. V. Romalis¹

¹*Department of Physics, Princeton University, Princeton, New Jersey 08544, USA*

²*Department of Geosciences, Princeton University, Princeton, New Jersey 08544, USA*

We describe an ultra-sensitive atomic magnetometer using optically-pumped potassium atoms operating in spin-exchange relaxation free (SERF) regime. We demonstrate magnetic field sensitivity of 160 aT/Hz^{1/2} in a gradiometer arrangement with a measurement volume of 0.45 cm³ and energy resolution per unit time of 44ħ. As an example of a new application enabled by such a magnetometer we describe measurements of weak remnant rock magnetization as a function of temperature with a sensitivity on the order of 10⁻¹⁰ emu/cm³/Hz^{1/2} and temperatures up to 420°C.

High sensitivity magnetometry is used in many fields of science, including physics, biology, neuroscience, materials science and geology. Traditionally low-temperature SQUID magnetometers have been used for most demanding applications, but recent development of atomic magnetometers with sub-femtotesla sensitivity has opened new possibilities for ultra-sensitive magnetometry [1].

Here we report new results of sensitive magnetic field measurements using a spin-exchange relaxation-free potassium magnetometer. By eliminating several sources of ambient magnetic field noise and optimizing operation of the magnetometer we achieve magnetic field sensitivity of 160 aT/Hz^{1/2} at 40 Hz. The measurement volume used to obtain this sensitivity is 0.45 cm³, resulting in a magnetic field energy resolution of $VB^2/2\mu_0 = 44\hbar$, a factor of 10 smaller than previously achieved with atomic magnetometers [2]. Energy resolution on the order of ħ has been realized with SQUIDs at high frequency and milli-Kelvin temperatures with small input coils [3, 4]. However for cm-sized SQUID sensors operating at 4.2 K the energy resolution at low frequency is typically several hundreds ħ [5, 6, 7] and the magnetic field sensitivity is about 1 fT/Hz^{1/2} [8].

When comparing various magnetometry techniques it is important to distinguish between applications requiring detection of smallest magnetic moments and those requiring detection of smallest magnetizations. For the former, it is usually advantageous to use the smallest possible sensor. For example, magnetic resonance force microscopy (MRFM) can detect a single electron spin [9]. On the other hand, for detection of very weak magnetization one needs a sensor with the highest magnetic field sensitivity, since $B \sim \mu_0 M$ in the vicinity of the source. For example, recently developed magnetometers using a single nitrogen-vacancy (NV) center in diamond are promising for detection of single electron and nuclear spins because of their small size [10, 11]. In diamond crystals with larger concentration of NV centers the magnetic field sensitivity is limited by dipolar interactions with other inactive color centers and has been optimistically projected at 10⁻¹⁶ T/Hz^{1/2}/cm^{3/2} [12], which is the level already realized experimentally in this work.

One of the well-developed magnetometry applications requiring high magnetization sensitivity is paleomagnetism [13]. Analysis of magnitude and direction of remnant magnetization in ancient rocks provides geological information going back billions of years and has been used, for example, to establish the latitudinal distribution of continents through time and to provide a critical test of the theory of plate tectonics. The magnetization is usually carried by low concentrations of tiny igneous crystals or sedimentary grains of magnetite or hematite, leading to very weak bulk magnetization. SQUID-based rock magnetometers are widely used for studies of such samples.

Here we demonstrate measurements of weakly-magnetized rock samples with higher sensitivity than possible with SQUID-based magnetometers [14]. Equally important, the measurements are performed continuously as a function of temperature with temperatures up to 420°C. Such temperature-dependent studies are crucial for paleomagnetic measurements as it allows one to separate the contribution of recently acquired magnetization and understand which magnetic minerals are present in the sample. In the past such measurements could only be obtained by repeated heating and cooling cycles of the sample or with much lower sensitivity using a variable temperature vibrating sample magnetometer [15]. Atomic magnetometry thus allows more sensitive magnetization measurements over a wider range of temperatures than is possible with any other detector.

The basic principles of spin-exchange relaxation free alkali-metal magnetometers have been described in [16, 17]. They are based on the observation that the dominant source of spin relaxation due to spin-exchange collision in alkali-metal vapor is suppressed at high alkali-metal density in a low magnetic field [18]. The fundamental sensitivity limits of such magnetometers due to spin projection noise are estimated to be on the order of 10⁻¹⁷ fT/Hz^{1/2}/cm^{3/2}. The main experimental challenge in achieving such sensitivity is to minimize ambient sources of magnetic field noise.

Superconducting shields can in principle provide a magnetic noise-free environment. However, in applica-

tions requiring measurements on samples above cryogenic temperature one is often limited by “dewar noise”- magnetic field noise on the order of several $\text{fT}/\text{Hz}^{1/2}$ generated by conducting radiation shields used for thermal insulation [19]. For this work we use a ferrite magnetic shield, first introduced in [20], as the inner-most shield layer. Low electrical conductivity of ferrite materials eliminates magnetic noise generated by Johnson currents allowing one to reach magnetic noise level below $1 \text{ fT}/\text{Hz}^{1/2}$. Other conducting materials in the vicinity of the magnetic sensor can also generate Johnson magnetic noise. We recently developed a new method based on fluctuations-dissipation theorem to estimate magnetic noise from conductors in various geometries [21]. It allows us to identify the largest sources of noise and select appropriate experimental components.

A drawing of the magnetometer apparatus is shown in Fig. 1. The sample, such as a weakly magnetized rock, is introduced through a 12 mm ID quartz tube that passes through the apparatus. The sample can be heated in-situ by electric heaters with AC current at 20 kHz. To reduce magnetic noise from the sample heating wires, they are removed from the vicinity of the magnetometer and heat is transmitted by diamond strips held with AlN cement. To thermally isolate the sample heater from the magnetometer a radiation shield is constructed by depositing a thin film of gold through a fine wire mesh on a glass slide. A spherical glass cell 23 mm in diameter containing K metal, 60 torr of N_2 and 3 atm of ^4He gas is heated to 200°C in a boron-nitride oven with AC electric heaters. Magnetic fields and first-order gradients are controlled by a set of coils wound on a G-7 fiberglass frame. The same frame also incorporates water cooling. The apparatus is enclosed in the ferrite magnetic shield with a diameter and length of 10 cm and operates in a vacuum of 1 mTorr. Not shown in the figure are a 316 stainless steel vacuum vessel and two additional layers of mu-metal magnetic shields.

The magnetometer is operated using 773 nm DFB lasers which are cooled to -20°C to reach K D1 line at 770 nm; no additional wavelength or intensity feedback is needed. The pump laser is tuned near the resonance and directed along the \hat{z} axis, while the probe laser is detuned by about 0.5 nm to the red side of the resonance and is sent along the \hat{x} axis. The polarization of the probe laser is measured using Faraday modulation technique. All three components of the magnetic field are zeroed and field gradients are adjusted to maximize the signal. Gradiometric measurements are performed by imaging the probe beam onto a two-channel photodiode and taking the difference between the two channels. The effective distance between the two channels, called the baseline of the gradiometer, is equal to 0.5 cm, determined by applying a calibrated magnetic field gradient. The distance between the sample and the sensor volume is equal to 2.4 cm, determined from the ratio of the signals in the

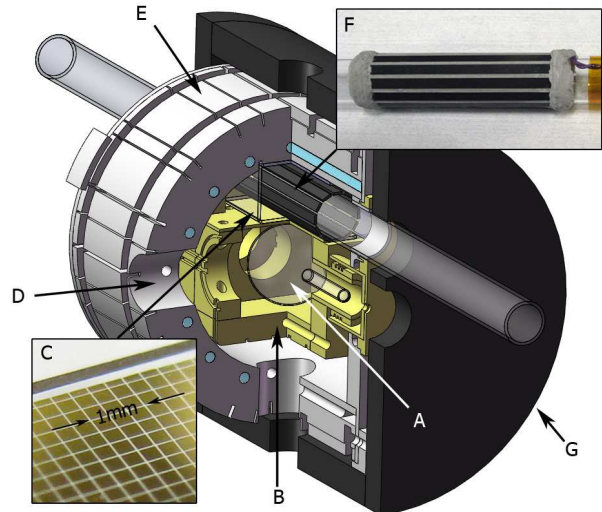


FIG. 1: Drawing of the magnetometer system. A- alkali-metal cell, B-boron-nitride oven, C- photo of the radiation shield, D- optical access for probe laser, E- G-7 fiberglass frame for magnetic field and gradient coils and water cooling, F - photo of the sample heater, G- ferrite magnetic shield.

two channels of the gradiometer. The sensing volume for each channel is $0.5 \times 0.5 \times 1.8 \text{ cm}^3$. Atom diffusion plays a minor role on the time scale of spin relaxation.

To understand the performance of the magnetometer we have developed a detailed model of the optical rotation signal that incorporates various relaxation effects for the K vapor and the absorption of the pump laser as it propagates into the optically-dense cell [22]. A plot of the optical rotation signal in response to a 10 pT low-frequency excitation field is shown in Fig. 2, comparing the results of the model and experimental measurements. The alkali-metal density and the resonance linewidth are measured independently, so there are no free parameters in the model. The overall size of rotation is in good agreement with predictions. The probe polarization rotation noise is about $1.5 \times 10^{-8} \text{ rad}/\text{Hz}^{1/2}$, limited by photon shot noise. So the sensitivity of the magnetometer can reach $5 \times 10^{-17} \text{ T}/\text{Hz}^{1/2}$ under optical conditions in the absence of any environmental magnetic noise.

In practice, to realize the lowest measured magnetic noise, we need to somewhat compromise the performance of the magnetometer to operate in the regime of lowest environmental magnetic noise. While the sensitivity of the magnetometer is largest for magnetic fields with a frequency below its natural bandwidth of about 3 Hz, the magnetic field noise increases at low frequency. This $1/f$ noise is due to hysteresis losses in the ferrite shield and is a feature of all magnetic materials [20]. The ferrite material used for the shield was chosen for its low loss factor. We introduce a bias B_z field to shift the magnetometer resonance and the peak of the magnetic field response to

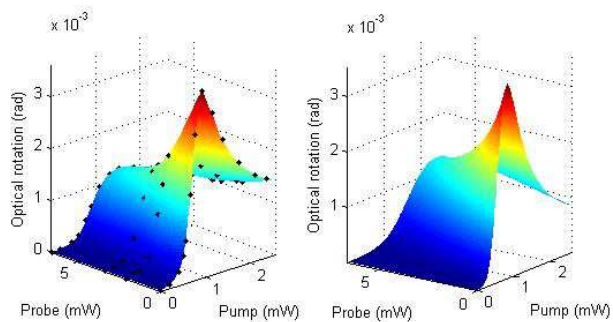


FIG. 2: Optical rotation in response to a 10 pT oscillating magnetic field as a function of the pump and probe laser power. Left panel - measurement points with color interpolation, right panel- theoretical calculation.

higher frequencies. Unfortunately, this technique reduces the magnetometer signal since only the co-rotating component of an oscillating magnetic field excites the spins.

In Fig. 3 we summarize the magnetic noise measurements. The data are recorded for several values of the bias field B_z and the magnetic field response is shown in the top panel. The bottom panel shows the magnetic field noise from a single magnetometer channel and the noise obtained from a gradient measurement. The noise in the difference of the two channels is divided by $\sqrt{2}$ to determine the intrinsic sensitivity of each channel. The optical rotation noise, recorded in the absence of the pump beam, is also shown. The intrinsic magnetic field noise obtained from the gradiometer measurements reaches 160 aT/Hz^{1/2} at 40 Hz. It is still not limited by optical rotation noise and is probably due to imperfect cancellation of the ferrite noise or local sources of magnetic fields, such as produced by droplets of K metal. The magnetization sensitivity of the gradiometer for our geometry with a 1 cm³ sample reaches 6×10^{-11} emu/cm³/Hz^{1/2}.

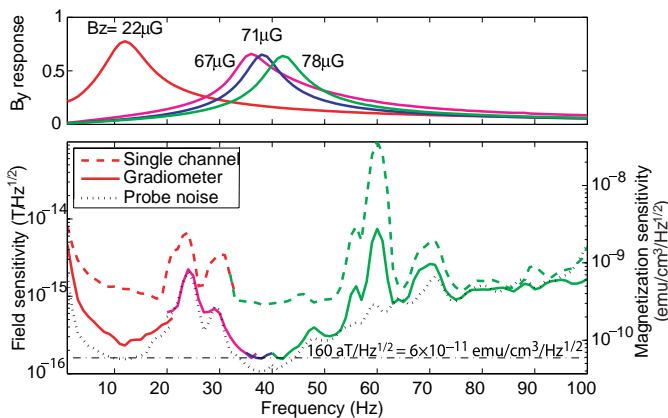


FIG. 3: Magnetic field response curves (top) and noise spectrum (bottom) for different values of the B_z magnetic field. The left axis shows magnetization sensitivity of the gradiometer.

The material samples are introduced into the apparatus through the access tube at ambient pressure. The sample is held at the end of high purity quartz tube by pumping on its other end with a vacuum pump. We found that all glues that we tested have a large magnetic contamination and most of them would not survive heating to required temperatures, while the quartz tube did not present significant background after thorough cleaning. The quartz tube and the sample are rotated around the axis at about 7 Hz to distinguish sample magnetic fields from constant backgrounds and move the signal to a region of lower magnetic field noise.

A 9 mm diameter, 13 mm long cylinder was prepared from a sample of very weakly magnetized ~ 635 Ma Ravensthorpe Formation peloidal Dolostone from the Mackenzie Mountains, Canada. Two vector components of the rock magnetization were determined by measuring the phase of the recorded signal relative to the sample rotation phase. The absolute value of the magnetization transverse to the rotation axis is plotted in Figure 4 as a function of temperature. The sample is continuously rotated and slowly heated over a period of about 2 hours. The magnetization drop at 300-350°C is due to unblocking of pyrrhotite or titanomagnetite crystals with the remaining magnetization most likely carried by magnetite. Measurements of all 3 vector components of the magnetization can allow one to obtain the direction of primary sedimentary magnetization.

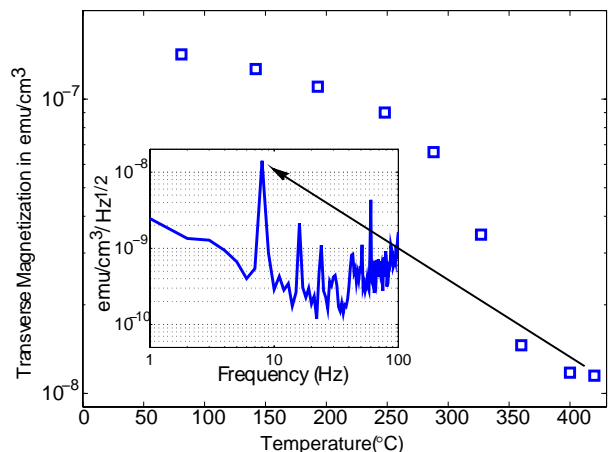


FIG. 4: Rock magnetization as a function of temperature. Inset shows that even at highest temperature the signal-to-noise is greater than 30. These measurements are obtained without gradiometric recording.

In summary, we have demonstrated what is to our knowledge the most sensitive cm-sized detector of magnetic fields and magnetization operating at low frequency. The absence of cryogenics allows for much larger thermal power dissipation, so sample temperatures can be varied over a wide range without extensive radiation shielding.

We have achieved sample temperatures up to 500°C and higher temperatures should be possible with thicker heating wires. Samples have also been maintained at room temperature by gently blowing air through the sample tube. The small size, low laser power and continuous magnetic field recording allow versatile use of the magnetometer. In addition to the paleomagnetic application explored here, many other uses can be readily implemented, including detection of magnetic nanoparticles [23], NMR [24] and weak high-temperature ferromagnetic ordering [25]. The fundamental sensitivity limits of SERF magnetometers have not yet been reached, so further improvements can be expected. We would like to thank John Tarduno for useful discussions. This work was supported by NSF grant PHY-0653433.

-
- [1] D. Budker and M. Romalis, *Nature Physics* **3**, 227 (2007).
 [2] I.K. Kominis, T.W. Kornack, J.C. Allred, and M.V. Romalis, *Nature* **422**, 596 (2003).
 [3] D.D. Awschalom *et al.* *Appl. Phys. Lett.* **53**, 2108 (1988).
 [4] M. Mück, J. B. Kycia, and J. Clarke, *Appl. Phys. Lett.* **78** 967 (2001).
 [5] D. Drung *et al.*, *IEEE Trans. Appl. Supercond.* **17**, 699 (2007).
 [6] P. Carelli, M. G. Castellano, *Physica B* **280**, 537 (2000).
 [7] P. Hakonen, M. Kiviranta, H. Seppä, *J. Low Temp. Phys.* **135**, 823 (2004).
 [8] D. Drung, *Physica C* **368**, 134 (2002).
 [9] D. Rugar, R. Budakian, H. J. Mamin and B. W. Chui, *Nature* **430**, 329 (2004).
 [10] J. R. Maze *et al.*, *Nature* **455**, 644 (2008).
 [11] G. Balasubramanian *et al.*, *Nature* **455**, 648 (2008).
 [12] J. M. Taylor *et al.*, *Nature Physics* **4**, 810 (2008).
 [13] *Paleomagnetic Principles and Practice*, Lisa Tauxe, Kluwer (2002).
 [14] J. L. Kirschvink, R. E. Kopp, T. D. Raub, C. T. Baumgartner and J. W. Holt, *Geochem. Geophys. Geosys.* **9**, Q05Y01 (2008).
 [15] M. Le Goff and Y. Gallet, *Earth and Planet. Sci. Lett.* **229**, 31 (2004).
 [16] J. C. Allred, R. N. Lyman, T. W. Kornack and M. V. Romalis, *Phys. Rev. Lett.* **89**, 130801 (2002).
 [17] I. M. Savukov and M. V. Romalis, *Phys. Rev. A* **71** 023405 (2005).
 [18] W. Happer and H. Tang, *Phys. Rev. Lett.* **31**, 273 (1973).
 [19] J. Nenonen, J. Montonen, and T. Katila, *Rev. Sci. Instrum.* **67**, 2397 (1996).
 [20] T. W. Kornack, S. J. Smullin, S.-K. Lee, and M. V. Romalis, *Appl. Phys. Lett.* **90**, 223501 (2007).
 [21] S.-K. Lee and M. V. Romalis, *J. Appl. Phys.* **103**, 084904 (2008).
 [22] T. G. Walker and W. Happer, *Rev. Mod. Phys.* **69**, 629 (1997).
 [23] Chemla Y.R. *et al.*, *PNAS* **97**, 14268 (2000).
 [24] Ledbetter M.P. *et al.* *PNAS* **105**, 2286-2290 (2008).
 [25] Young D.P. *et al.* *Nature* **397**, 412 (1999).